Revision

Electrochemically Driven C-H Hydrogen Abstraction Processes with the Tetrachloro-Phthalimido-N-Oxyl (Cl_4PINO) Catalyst

Mark A. Buckingham,[a] William Cunningham,[a] Steven D. Bull,[a] Antoine Buchard,[a] Andrea Folli,[b] Damien M. Murphy,[b] Frank Marken[a]*

[a] Department of Chemistry, University of Bath, Claverton Down, Bath BA2 7AY, UK

[b] School of Chemistry, Cardiff University, Cardiff CF10 3AT, UK

To be submitted to Electroanalysis

Proofs to F. Marken (F.Marken@bath.ac.uk)

Abstract

The radical redox mediator tetrachloro-phthalimido-N-oxyl (Cl_4PINO) is generated at a glassy carbon electrode and investigated for the model oxidation of primary and secondary alcohols with particular attention to reaction rates and mechanism. The two-electron oxidation reactions of a range of primary, secondary, and cyclic alcohols are dissected into an initial step based on C-H hydrogen abstraction (rate constant k_1, confirmed by kinetic isotope effect) and a fast radical-radical coupling of the resulting alcohol radical with Cl_4PINO to give a ketal that only slowly releases the aldehyde/ketone and redox mediator precursor back into solution (rate constant k_2). *In situ* electrochemical EPR reveals Cl_4PINO sensitivity towards moisture. DFT methods are applied to confirm and predict C-H hydrogen abstraction reactivity.

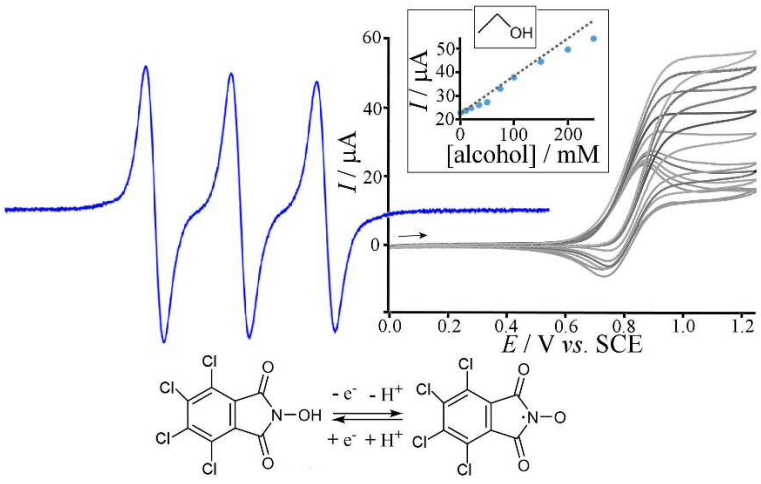

KEYWORDS: C-H abstraction; voltammetry; redox mediator; TEMPO; radicalisation; fuel.

Introduction

Radical organocatalysts such as phthaloimido-*N*-oxyl (PINO), produced by one-electron oxidation of *N*-hydroxy-phthaloimide, provide prominent examples of versatile reagents [1,2] that can be generated *in situ* for example at electrode surfaces [3,4]. A diverse range of oxidation and functional group exchange reactions are possible [5] including oxidation of lignin model compounds [6]. The class of these organocatalyst reagents also includes TEMPO [7] and TEMPO derivatives [8-10]. A comparison of TEMPO reactivity versus PINO reactivity has been reported for alcohol oxidation [11] and for cellulose oxidation [12]. The tetrachloro-derivative of phthaloimido-N-oxyl (Cl_4PINO [1] see Reaction Scheme 1) has attracted particular attention based on the ability to perform benzylic and allylic C-H hydrogen abstraction [13] with the benefit of fragile carbon structures (e.g. in α-pinene) being retained and converted directly into valuable products (e.g. to verbenone). A synthesis for Cl_4PINO and derivatives was reported in 2005 by Sugamoto and coworkers [14].

In 1987 Matsui and coworkers [15] presented a detailed study of the kinetics and catalytic reactivity of the PINO radical. PINO was also investigated in the context of lignin model reagent oxidation to develop lignin conversion into useful products [16]. Rafiee et al. reported a detailed study directly comparing the reactivity of TEMPO and PINO for alcohol oxidations [11]. In 1998 Gorgy and coworkers demonstrated oxidation of primary and secondary alcohols with phthalimido-*N*-oxyl mediators including the tetrachloro derivative Cl_4PINO [17]. This study established the formation of aldehyde products from both types of substrates under anaerobic

conditions (with oxygen present also carboxylates were formed) as well as providing voltammetry data and significant insight into the reactivity and degradation of the Cl_4PINO intermediate. This system is revisited here as a model case with emphasis on quantitative mechanistic analysis and DFT prediction of reaction rates and pathways.

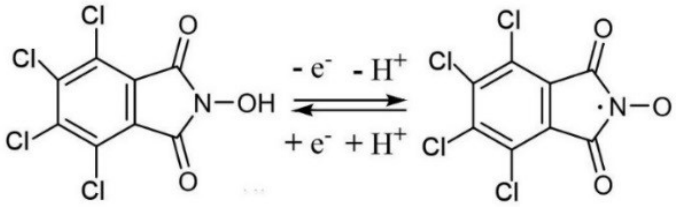

Reaction Scheme 1. One-electron oxidation of tetrachloro-*N*-hydroxyl-phthalimide (Cl_4NHPI) to tetrachloro-phthalimido-*N*-oxyl (Cl_4PINO).

Wertz and Studer [18] provide a review of NO-radical reagents and their applications in green oxidations, in particular in reactions driven by atmospheric oxygen [19-21]. Xu and coworkers demonstrated the C-H hydrogen abstraction for ethylbenzene and similar hydrocarbon substrates [22]. Most mechanistic studies to date have been undertaken on the parent PINO radical. The considerable O-H bond dissociation energy of NHPI [23] (375 ± 10 kJ mol^{-1}) has been shown to lead to mildly exothermic C-H hydrogen abstraction reactions. Considerable kinetic isotope effects of $k_H/k_D \approx 11.8$ for benzhydrol, and $k_H/k_D \approx 17$-28 for benzyl alcohol, ethylbenzene, benzaldehyde and toluene were reported for PINO reactions [24]. A relationship based on Marcus theory has been suggested to explain these high kinetic isotope effects close to the limit of thermo-neutral reactions (consistent with a strong H-tunnelling contribution).

This report offers new quantitative insights into Cl_4PINO reactivity at electrode surfaces. *In situ* electrochemical EPR is employed to detect the radical. Reactivity towards primary alcohols (ethanol, 1-octanol, 2-phenylethanol, 2-nitroethanol, benzylalcohol) and towards secondary alcohols (2-propanol, 3-pentanol, 1-phenylethanol, cyclo-hexanol, cyclo-pentanol) is reported including a quantitative (based on computer simulation of voltammetric current responses) analysis of reactions steps and rate constants. Experimental data are correlated to DFT activation barrier calculations. Consistent with literature reports, the rate constant for C-H hydrogen abstraction is shown to be high for electron-rich secondary alcohols and for aromatic substituents. The kinetic isotope effect for d_5-ethanol is shown to be very high with = 15.

Experimental

Reagents. The catalyst precursor *N*-hydroxy-tetrachloro-phthalimide (CAS Number 85342-65-0, ALD00564 Aldrich) was synthesised following a literature procedure [1]. Acetonitrile (HPLC quality), ethanol (ACS quality) and 2-propanol (ACS quality) were all purchased from VWR chemicals and used as received. Tetrabutylammonium hexaflourophosphate (electrochemical grade, ≥ 99.0%), 3-pentanol (98%), 1-phenylethanol and 2-phenylethanol (both ≥ 99.0%), 1-octanol (≥ 99%), 2-nitroethanol (98%), cyclohexanol (98%), cyclopentanol (98%), benzylalcohol (98%), and pyridine (ACS reagent) were purchased from Sigma-Aldrich and used without further purification.

Instrumentation. Electrochemical measurements were performed with an Ivium Compactstat (Ivium, Netherlands) in a three-electrode configuration (working electrode 3 mm diameter glassy

carbon (BAS Ltd.), counter electrode platinum wire, reference electrode aqueous KCl-saturated calomel (SCE) pre-equilibrated in acetonitrile). Continuous wave (CW) X-band (9.5 GHz) EPR spectra were recorded on a Bruker EMX-micro spectrometer equipped with a Bruker ER4122 SHQE-W1 super high Q resonator, operating at 100 kHz field modulation. The EPR spectra were recorded at room temperature. The measurement cell used consisted of a quartz *in situ* electrochemical flat cell, using a Pt plate working electrode, Pt wire counter electrode and a silver wire pseudo-reference electrode.

Procedure for Electrocatalysis Experiments. For each of the electrocatalysis voltammetry experiments, Cl_4NHPI pre-catalyst (6 mg) and NBu_4PF_6 electrolyte (0.22 g) were weighed and dissolved in acetonitrile (20 mL). Pyridine (1.6 mL; 1 M) was then added and a cyclic voltammogram was recorded to determine the initial concentration of Cl_4NHPI pre-catalyst. Then alcohol substrate was added in increments and cyclic voltammetry experiments were performed (scan rate 100 mVs^{-1}, E step of 1 mV, potential range 0.0 V to +1.25 V vs. SCE).

Procedure for Computer Simulation of Voltammetric Data. The simulation of cyclic voltammetry data was performed employing DigiElch 4.F software assuming a semi-infinite 1D finite diffusion model. Diffusion coefficients were either determined experimentally (*vide infra*) or estimated with the Wilke-Chang expression [25].

Procedure for Computer DFT Methods. Calculations were performed with Gaussian09 suites of code [26] and protocol rB3LYP/6-311++G(d,p)/SCRF= (cpcm,solvent= acetonitrile)/

temperature= 298.15. The nature of all the stationary points as minima or transition states was verified by calculations of the vibrational frequency spectrum. All transition states were characterised by normal coordinate analysis revealing precisely one imaginary mode corresponding to the intended reaction. Full details, including coordinates for all stationary points, computed free enthalpies and vibrational frequency data, as well as summary tables can be found in the data section.

Results and Discussion

One-Electron Formation of Tetrachloro-Phthalimido-*N*-Oxyl (Cl_4PINO) Radicals. Consistent with literature reports [17], Cl_4NHPI is oxidised in a one-electron process (see Reaction Scheme 1). Figure 1A shows typical cyclic voltammograms obtained at a 3 mm glassy carbon electrode in acetonitrile with 0.05 M NBu_4PF_6 supporting electrolyte. A quasi-reversible oxidation occurs with $E_{1/2}$ = ½ (E_{ox} + E_{red}) = + 1.27 V *vs.* SCE. Peaks appear broad in particular at higher scan rate as has been reported by Gorgy [17]. Attempts to perform rotating disc voltammetry with this system failed, probably due to strong interaction of the radical oxidation product Cl_4PINO with the glassy carbon electrode surface (*vide infra*). In order to obtain an estimate for the number of electrons transferred in this process, the diffusion coefficient for Cl_4NHPI was initially estimated (employing the Wilke-Chang approximation [25]) as $D \approx 1.57 \times 10^{-9}$ m^2 s^{-1}. With this information and employing the Randles-Sevcik equation (see equation 1) [27], it is then possible to obtain an estimate for the number of electrons transferred for each molecule diffusing to the electrode surface, n = 0.8, consistent with a one-electron process.

$$I_p = (2.69 \times 10^5)\, n^{3/2} A c \sqrt{D \nu} \qquad (1)$$

Here, I_p is peak current (A), F is the Faraday constant (C mol^{-1}), A is the electrode area (m^2), c denotes the bulk concentration of the diffusing species (mol m^{-3}), D is the diffusion coefficient (m^2 s^{-1}), ν is the scan rate (V s^{-1}), R is the gas constant (J K^{-1} mol^{-1}), and T denotes the absolute temperature (K). The reversibility of the cyclic voltammogram can be significantly improved with addition of pyridine into the solution (or collidine as was reported by Gorgy et al. [17]). Figure 1B shows the effect of adding 0.1 mM and 1 mM pyridine into a solution of 1 mM Cl_4NHPI. The oxidation response identified as formation of Cl_4PINO diminishes and a new more reversible voltammetric signal is observed at a less positive potential. The presence of two distinct oxidation peaks in Figure 1B suggests that pyridine might either act as buffer (which is depleted to give the second oxidation peak), or it may also form a complex with Cl_4NHPI to then give the pyridinium upon oxidation. The exact nature of the type of electron transfer may depend on pyridine concentration. This redox process is detected with $E_{1/2}$ = 0.82 V *vs*. SCE in the presence of 1 M pyridine. The plot in the inset of Figure 1C shows scan rate dependent data obtained for oxidation of 1 mM Cl_4NHPI in the presence of 1 M pyridine. The plot is indicative of a diffusion-controlled process and the Randles-Sevcik equation (see equation 1) is employed again to obtain a more precise experimental value for the diffusion coefficient (now much lower in the presence of 1 M pyridine possibly indicative of complex formation) $D = 0.72 \times 10^{-9}$ m^2 s^{-1}. This value will be employed below in digital simulation analysis of voltammetric data. This digital simulation analysis has been limited to rate constants for chemical reaction steps with any further complexity due to effects from proton-coupled electron transfer being disregarded.

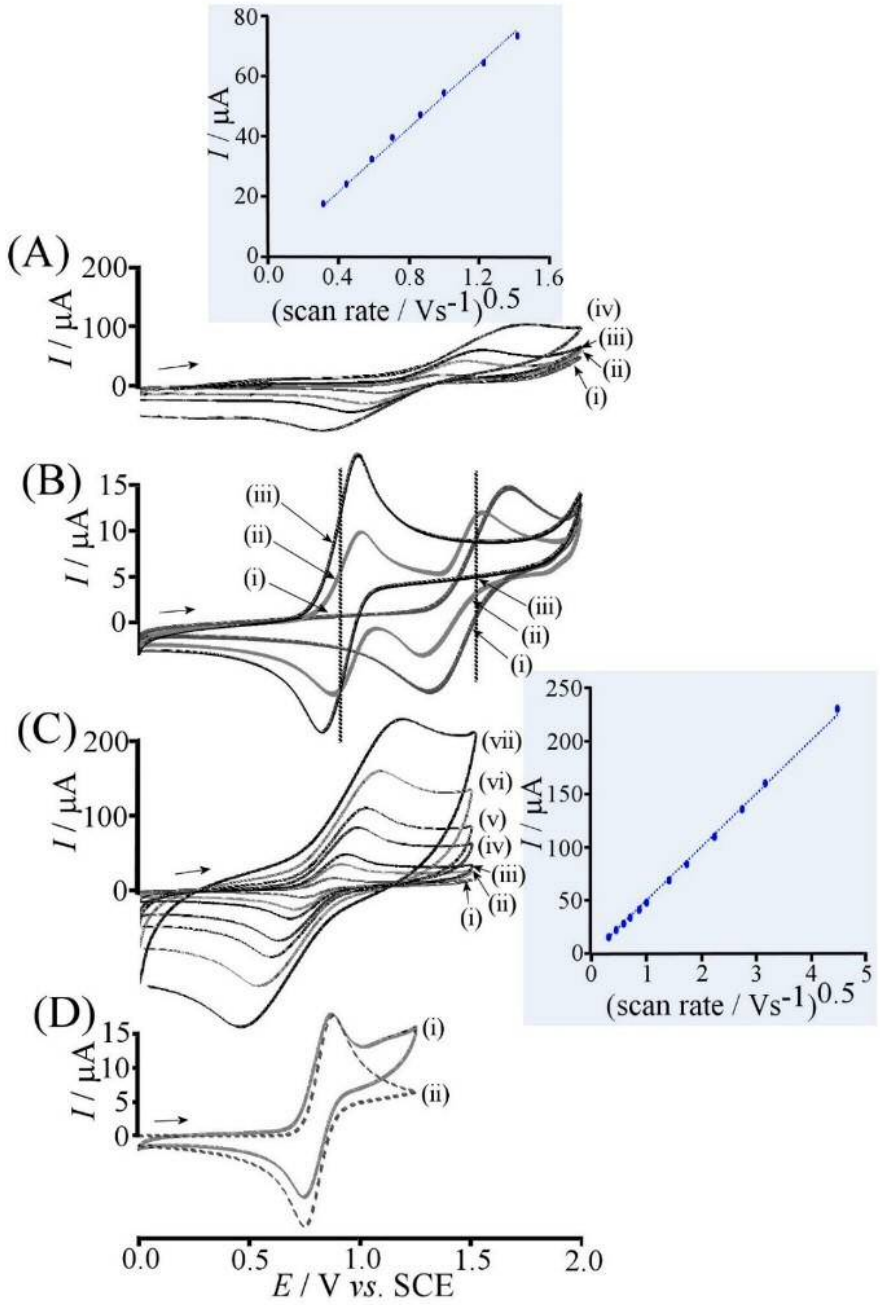

Figure 1. (A) Cyclic voltammogram (scan rate (i) 0.1 V s^{-1}, (ii) 0.5 V s^{-1}, (iii) 1 V s^{-1}, (iv) 3 V s^{-1}) for 1 mM Cl_4NHPI in acetonitrile (0.05 M NBu_4PF_6). Inset: plot of I_p *vs.* (scan rate)$^{1/2}$ with a line of best fit. (B) Cyclic voltammagrams (scan rate 0.1 V s^{-1}) for the oxidation of 1 mM Cl_4NHPI in acetonitrile (0.05 M NBu_4PF_6) with added pyridine (with (i) 0, (ii) 0.1, (iii) 1 mM pyridine). (C) Cyclic voltammograms (scan rate (i) 0.1 Vs^{-1}, (ii) 0.5 Vs^{-1}, (iii) 1 Vs^{-1}, (iv) 3 Vs^{-1}, (v) 5 Vs^{-1}, (vi) 10 Vs^{-1}, (vii) 20 Vs^{-1}) for oxidation of 1 mM Cl_4NHPI in acetonitrile (0.05 M NBu_4PF_6, 1 M pyridine). Inset: plot of I_p *vs.* (scan rate)$^{1/2}$ with a line of best fit. (D) Experimental (solid line) and simulated (hashed line) cyclic voltammogram (scan rate 0.1 V s^{-1}, 1.25 mM concentration, 1 M pyridine) for the oxidation of Cl_4NHPI.

Next, *in situ* electrochemical EPR analysis (compare previous non-electrochemical EPR experiments for related radical species) [28,29] is employed to explore the reactivity of the Cl_4PINO radical intermediate. Figure 2Ai shows the background without applied potential with a solution of 1 mM Cl_4NHPI showing no radical species. The oxidation was carried out in a flat-cell at a platinum flag electrode. Figure 2Aiii shows that a well-defined three-line spectrum, composed of a 1:1:1 triplet, (with g_{iso} = 2.0074 and a_{iso} = 12.36 MHz or 4.41 G) is observed. This signal is consistent with previously reported EPR spectra of other phthalimido-*N*-oxyl derivatives [28]. The EPR spectrum recorded in the presence of ambient oxygen (see Figure 2Aii) are broadened and less intense compared to the spectrum recorded in anaerobic conditions (see Figure 2Aiii). Paramagnetic triplet O_2 is well-known to weakly interact with both, closed-shell [30] or open-shell organic molecules. It can be hypothesised that collision/magnetic interaction of dioxygen with Cl_4PINO could cause broadening of the EPR signal. For solutions saturated with triplet O_2, there could be enough mixing between the O_2 spin and the nitroxide spin to cause extensive broadening (*i.e.*, Heisenberg broadening so severe that it could cause the complete disappearance of the signal) [31].

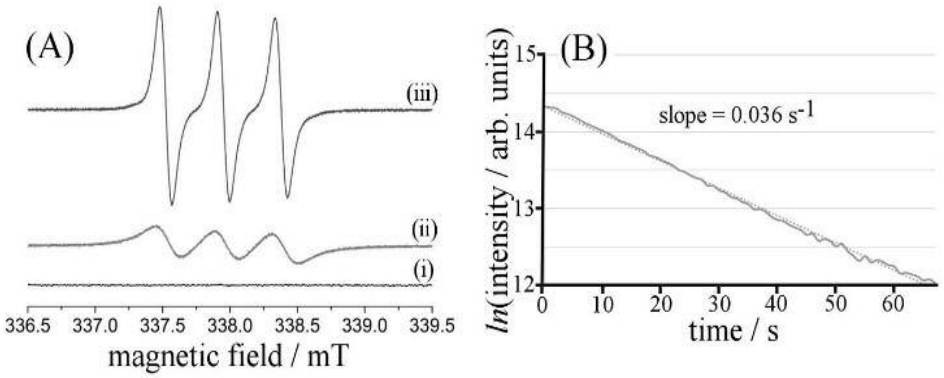

Figure 2. (A) CW X-band EPR spectra (room temperature, at 100 kHz modulation frequency, 1 Gauss modulation amplitude, 18.9 mW microwave power and $5.02 \cdot 10^4$ receiver gain) of 1 mM Cl_4NHPI in acetonitrile with 1 M pyridine and .05 M NBu_4PF_6 (i) before electrolysis, (ii) during anodic electrolysis in the presence of air, (iii) during anodic electrolysis de-aerated with nitrogen. (B) Logarithmic plot of EPR signal intensity of the central line, I(0), *vs.* time.

The relative intensities of the EPR lines can also provide valuable information about the anisotropy of the radical motion within the fast motion regime, *i.e.,* where the rotational correlation time τ_c (the reciprocal of the frequency of rotation) associated with rotational diffusion of the molecule is < 2 ns. In this regime, τ_c can be defined according to equation 2 [32,33].

(2)

In Equation 2, $\Delta H(0)$ is the peak-to-peak line width in Gauss of the central line, and $I(+1)$, $I(0)$ and $I(-1)$ are the signal amplitudes of the low field, middle and high field lines respectively of the ^{14}N hyperfine components. In the case of Cl_4PINO, τ_c is in the order of a few tens of picoseconds, indicating fast rotation of the molecule in solution. In the narrower spectrum (Figure 2Aiii**)** the signal amplitude of the three lines decreases monotonically from low field to high field. This corresponds to an anisotropy parameter, ε equal to - 0.7, where ε is a dimensionless parameter, described in equation 3 [33].

(3)

If the long molecular axis is parallel to the N–O bond of the nitroxide radical, ε becomes increasingly negative with increased anisotropy of rotation. The negative character of the anisotropy parameter would also suggest that rotation along the axis parallel to the N–O bond is the fastest [32]. Figure 2B shows the transient of the signal intensity of the EPR central line, $I(0)$, versus time, recorded after switching off the electrolysis. Without new Cl_4PINO radicals being generated, a rapid decay of the signal intensity is observed with first order characteristics. Intentionally added water was observed to (at least qualitatively) lead to even faster decay. It seems therefore likely that moisture in the organic solvent system is a crucial factor in the slow decay of the Cl_4PINO radical species. Decay products such as dimers and trimers have been reported [15] and a previously suggested decay mechanism via radical disproportionation and hydrolytic attack on the cation appears plausible. For ambient levels of water (here estimated as 10-20 mM) the half-life of 28 s can be extracted. This corresponds to a relatively slow process when compared to voltammetry experiments which are typically an order of magnitude faster in time domain. It is therefore assumed that decay of the Cl_4PINO radical does not significantly contribute to the phenomena measured by cyclic voltammetry. However, it has to be kept in mind that moisture at higher levels could play a part in the mechanism and it could affect the mechanisms and rate constants.

The reversible voltammetric response for the oxidation of Cl_4NHPI can be analysed more quantitatively with the help of digital simulation tools (here the software package DigiElch 4.F is employed). Figure 1D shows a comparison of experimental data and simulation data for the oxidation of pre-catalyst Cl_4NHPI in the presence of 1 M pyridine. Although a good match is seen for the scan towards positive potentials, there is an unexpectedly lower peak response for the scan

towards negative potentials. This is attributed here to minor convection effects that displace the peak current slightly. An additional oxidation response at potential higher than +1 V *vs*. SCE can be tentatively attributed to additional glassy carbon surface processes in the presence of Cl_4PINO.

Two-Electron Catalytic Oxidation of Primary and Secondary Alcohols: Experiment. When oxidised, Cl_4NHPI is converted into the Cl_4PINO radical, which is known to be a potent C-H hydrogen abstraction reagent, for example for the oxidation of alcohols to aldehydes of ketones [17], but also for the conversion of CH-allylic carbon skeletons into α,β-unsaturated ketones without structural rearrangement [13]. Here, primary and secondary alcohol oxidation serves as a model system to provide new insights into the mechanism. Figure 3A shows a set of cyclic voltammograms for the oxidation of 1.25 mM Cl_4NHPI in acetonitrile and in the presence of 1 M pyridine (under argon). The addition of ethanol can be seen to lead to an increase in the anodic current and a concurrent decrease in the cathodic current, consistent with the voltammetric features for a catalytic process based on Cl_4PINO acting as a reactive intermediate.

The anticipated characteristics for an EC'-catalytic electrode process at low substrate concentration are associated with a linear increase (diffusion controlled) in anodic current with substrate/alcohol concentration. The inset in Figure 3A shows that this expected trend is indeed observed with a deviation (towards lower currents) only at higher ethanol substrate concentrations. In the limit of pure kinetic control an approximate analytical equation [11], $I_{cat} = nFA$ [catalyst] $(D\ k_1$ [alcohol]$)^{0.5}$, could be employed for approximate data analysis. A dependence of I_{cat} on the square root of substrate concentration is predicted. Here, the use of digital simulation allows

further mechanistic details to be resolved and distinct behavior for different alcohols to be interpreted. It is interesting to note that data analysis based on the simple equation for I_{cat} (in contrast to full simulation analysis) would give similar trends in rate constants but generally under-estimate their magnitude (*vide infra*). Figures 3B and 3C summarise data plots for anodic current maxima *versus* alcohol concentration for cyclopentanol, ethanol, octanol, 2-phenylethanol, 2-nitroethanol, benzylalcohol, 1-phenylethanol, cyclohexanol, 2-propanol and 3-pentanol. All data plots follow similar trends although clear differences are noted for different classes of alcohols. Data points represent experimental currents and dashed lines represent trends from digital simulation.

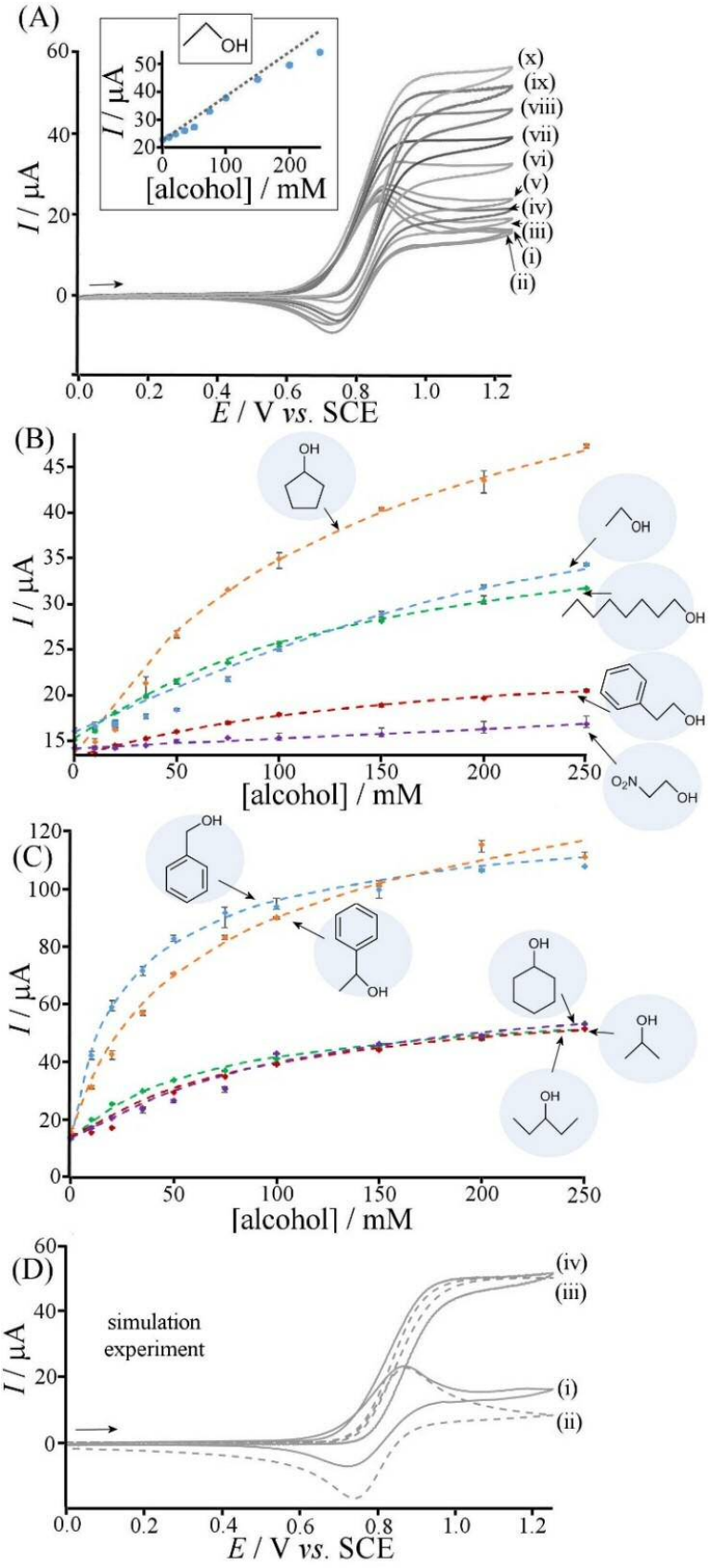

Figure 3. (A) Cyclic voltammograms (scan rate 0.1 Vs^{-1}, under argon) in acetonitrile with 1 M pyridine (0.05 M Bu_4NPF_6) for the oxidation of 1.25 mM Cl_4NHPI in the presence of (i) 0, (ii) 10, (iii) 20, (iv) 35, (v) 50, (vi) 75, (vii) 100, (viii) 150, (ix) 200, (x) 250 mM ethanol. Inset: plot of I_p *vs.* ethanol concentration. (B) Plot of I_p *vs.* alcohol concentration for cyclopentanol, ethanol, octanol, 2-phenylethanol, and 2-nitroethanol (dashed lines based on simulation). (C) Plot of I_p *vs.* alcohol concentration for benzylalcohol, 1-phenylethanol, cyclohexanol, 2-propanol, and 3-pentanol (dashed lines based on simulation). (D) Comparison of experimental (solid line) and simulation (dashed line) voltammetry data for the oxidation of 1.25 mM Cl_4NHPI in the absence and in the presence of 250 mM ethanol.

One emerging pattern from these data is the observation that phenyl-substituted and secondary alcohols react with a faster rate constant (the initial slope of current versus alcohol concentration is higher). A further significant trend is that all data plots converge towards a plateau at higher concentrations of alcohol. Therefore, something happens during the reaction that causes a depletion of the reactive Cl_4PINO species close to the electrode surface thereby suppressing the catalytic redox cycling and causing a current plateau (and not a square root dependence). Based on the much shorter time scale for the voltammetric experiment compared to the hydrolytic decay of the radical observed in EPR, the decay can be ruled out as a factor in the voltammetric characteristics (*vide supra*). Koshino et al. [37] suggested the hypothesis of the fast "capture" of hydrocarbon radicals with PINO radicals. Here, the Cl_4PINO radical concentration locally at the electrode surface is high and capture by dioxygen is unlikely. Therefore, a hypothetic capture mechanism is suggested based on the Cl_4PINO radical reacting with the alcohol radical intermediate (see Reaction Scheme 2), which under electrochemical conditions appears likely compared to the dioxygen capture process [8]. This hypothetical mechanism also helps maintaining the two-electron nature of the process. Similar reaction pathways have been observed for TEMPO mediated processes [32]. The mechanistic hypothesis is confirmed here by quantitative digital simulation, although there is currently no direct experimental proof for the short-lived hemi-ketal intermediate.

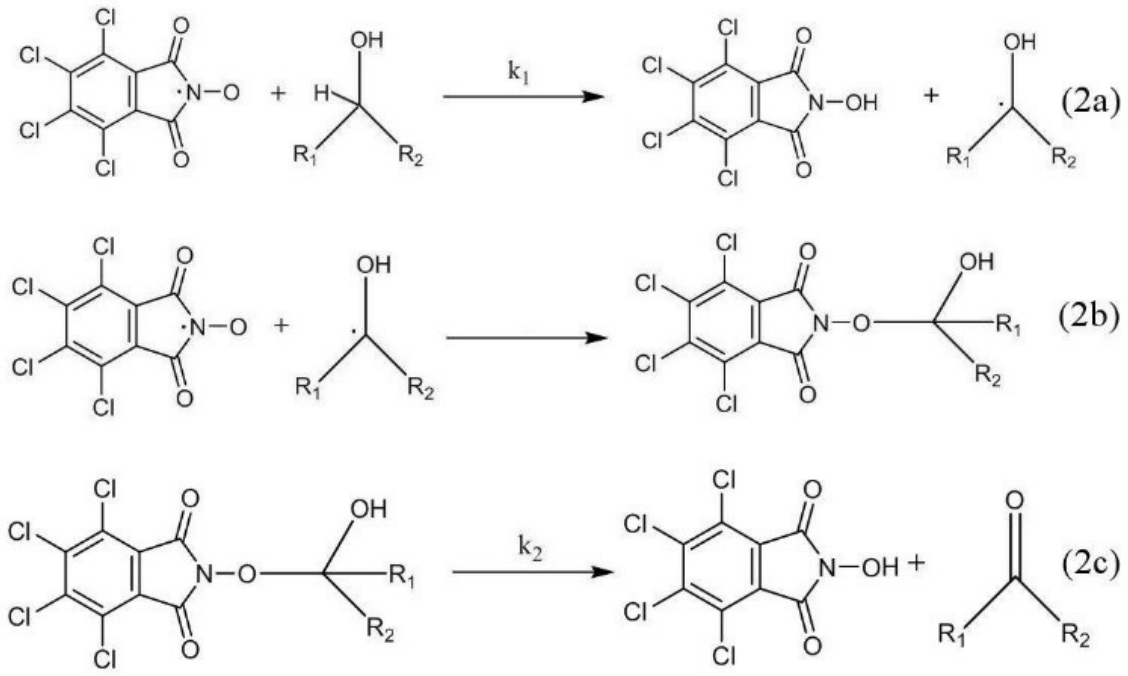

Reaction Scheme 2. Reaction of Cl_4PINO with alcohol (2a) and diffusion – controlled follow-up reaction (2b) leading to only half of the catalyst being recycled electrochemically. A slow hydrolytic step (2c) occurs outside of the diffusion layer at the electrode surface.

Two-Electron Catalytic Oxidation of Primary and Secondary Alcohols: Simulation. In Figure 1D it was demonstrated that quantitative digital simulation can be applied to the case of the reversible one-electron oxidation of Cl_4NHPI to Cl_4PINO. Next, a full simulation model for the alcohol oxidation was developed. The diffusion coefficients for alcohols in acetonitrile were estimated by employing the Wilke-Chang expression [25] (see Table 1). The simulation of anodic current data based only on equation 2a in Reaction Scheme 2 (with second order rate constant k_1) results in a straight line increase in current with lower substrate concentration. At high alcohol substrate concentrations currents follow a square root [alcohol]$^{0.5}$ dependence, which is consistent with EC'-catalysis. However, this square root trend does not fully account for the observed experimental data. At even higher alcohol concentrations a current plateau is observed. Therefore, the reaction in equation 2b needed to be introduced in addition to equation 2a to better account for

the shape and the plateau (and the removal of Cl_4PINO from the diffusion layer) at higher substrate concentration. The rate constant for this radical-radical coupling reaction was assumed to be diffusion controlled (set very high to not affect the results in the simulation). However, the follow-up reaction releasing the product (see equation 2c in Reaction Scheme 2 with rate constant k_2, here expressed as first order rate constant) is important and responsible for the observed magnitude of the plateau current (recapture of Cl_4NHPI from outside the diffusion layer) in the high substrate concentration limit.

Figure 3D shows a comparison of experimental data and simulation data. In the absence of substrate only the reversible current response is observed for the experiment (Figure 3Di, solid line) and for the simulation (Figure 3Dii, dashed line). In the presence of substrate, the anodic current is increased to a plateau with reasonably good agreement of experiment (Figure 3Diii, solid line) and simulation (Figure 3Div, dashed line). The additional hysteresis in the experimental voltammogram may be due to protons being generated during the alcohol oxidation (causing a local pH drift at the electrode surface). The simulation of the data allows two rate constants, k_1 and k_2, to be extracted for most alcohols (see Table 1).

Table 1. Summary of simulation data for Cl_4PINO catalysed oxidation of alcohols with rate constants k_1 and k_2 evaluated. Also shown are the DFT computed free energy activation barriers for the C-H hydrogen abstraction step from various alcohols by Cl_4PINO radical.[a]

ROH	k_1 / mol^{-1} dm^{3}s^{-1}	k_2 / s^{-1}	D / m^{2}s^{-1}	E_A / kJ mol^{-1}
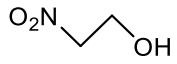	2.2	/	3.0 x 10^{-9}	107.8
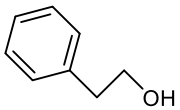	15	0.6	2.1 x 10^{-9}	96.1
	19	9	3.6 x 10^{-9}	92.5
	30	2.7	1.8 x 10^{-9}	90.7
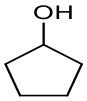	58	11	2.4 x 10^{-9}	85.9
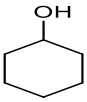	70	15	2.2 x 10^{-9}	88.3
	75	10	3.0 x 10^{-9}	84.6
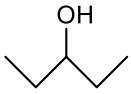	110	8	2.3 x 10^{-9}	85.6
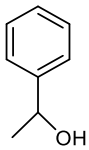	335	39	2.1 x 10^{-9}	77.5
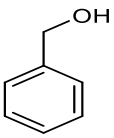	950	32	2.3 x 10^{-9}	78.4

[a] Protocol: B3LYP/6-311++g(2d,p)/298.15K/cpcm=acetonitrile. Activation barriers were calculated here as $E_A = \Delta G = G_{TS} - (G_{alcohol} + G_{radical})$.

In addition to quantifying the rate constants and confirming the mechanism, the digital simulation tool can be employed to confirm the effect of the Cl_4NHPI catalyst concentration. Additional experiments were performed (not shown) for 2-propanol and for ethanol for both 1.25 mM and 2.5 mM Cl_4NHPI catalyst precursor concentrations. The match between experimental data (points) and simulation (dashed line) is excellent without any change in parametrisation confirming the validity of the analysis and the suggested mechanism. General trends are identified such as (i) primary alcohols react slower (k_1 lower) compared to secondary and aromatic alcohols and (ii) the hydrolytic process (k_2) appears faster for benzylic systems and slow for 2-phenylethanol.

The effect of water on the reaction kinetics was investigated only at qualitative level (going from 10 mM to 100 mM and 1000 mM water) and changes in both initial slope and plateau current were observed for plots of anodic current versus alcohol concentration (for the oxidation of 2-propanol, not shown). This confirms the observed sensitivity of Cl_4PINO towards moisture (observed in the *in situ* electrochemical EPR as noted above). For the related N-hydroxyphthalimide / phthalimido-*N*-oxy system the reaction with water has been suggested to lead to inactive dimers [35] or trimers [36].

Two-Electron Catalytic Oxidation of Alcohols: Kinetic Isotope Effect. A further test for the validity of the data extracted for rate constant k_1 can be based on the kinetic isotope effect. Kinetic

isotope effects have been reported to be high for the redox mediator phthalimido-*N*-oxyl. For the hydrogen abstraction reaction, a classic isotope effect when replacing ethanol with d_5-ethanol (where = 1.41) would be expected to be approximately up to 7. However, tunnel effects for H-atom abstraction can significantly increase the effect and reported values for phthalimido-N-oxyl reactions range from 12 – 26 [37-40].

Experiments were carried out to contrast the rate of oxidation of ethanol with that of d_5-ethanol in acetonitrile with 1 M pyridine (0.05 M NBu_4PF_6 under argon). Figure 4 shows a plot of the anodic current *versus* substrate concentration and the change in the rate of oxidation is clearly revealed. However, a $k_{1,D}$ of 1.25 mol^{-1} dm^3 s^{-1} was found for d_5-ethanol, which when compared to $k_{1,H}$ of ethanol (= 19 mol^{-1} dm^3 s^{-1}), gives a kinetic isotope effect of 15. This result is in excellent agreement with literature reports on kinetic isotope effects for related C-H abstraction reactions[37] and it confirms the assignment of k_1 as the C-H hydrogen abstraction step in the reaction scheme.

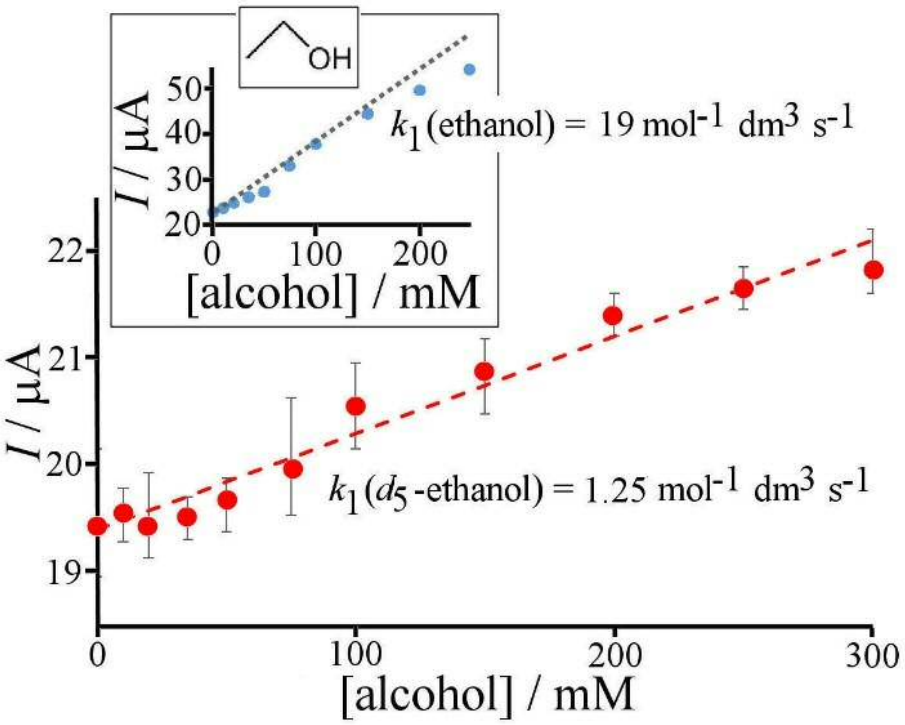

Figure 4. Plot of anodic peak current I_p *vs*. concentration of d_5-ethanol. Experimental data (points) are compared to simulated data (hashed) for a k_1 = 1.25 mol^{-1} dm^3 s^{-1}. Inset: for comparison plot of anodic peak current I_p *vs*. concentration of ethanol with k_1 = 19 mol^{-1} dm^3 s^{-1}.

Two-Electron Catalytic Oxidation of Primary and Secondary Alcohols: DFT Simulation. Computational methods allow sets of kinetic data to be correlated in a more systematic manner and to extract underlying mechanistic causes for the rate of reactions. This is of interest in particular for C-H abstraction reactions, which are dominated by molecular electronic factors. Recently, some of us investigated by DFT calculations [10] the related reaction between various primary alcohols and a derivative of the TEMPO$^+$ cation in $NaCO_3^-$ aqueous buffer, which was shown to likely proceed via a hydride transfer concerted step. Here, in contrast, the neutral Cl_4PINO radical is involved in an H-atom transfer instead. The case of H-atom transfer is usually affected by tunnelling and therefore would require more extensive calculation similar to those applied related gas phase reactions [41]. However, in this study only energy barriers are

determined/correlated and not absolute rate constants. The tunnelling effect impacts on the pre-exponential factor [40] and not on the energy barrier and it is assumed here that similar tunnelling effects occur for a range of different alcohol substrates.

Computational methods were used to model the mechanism of C-H abstraction from primary and secondary alcohols by the Cl_4PINO radical, first to correlate theory with experimental data, and ultimately to predict k_1 for a wider range of alcohols. The calculations revealed that the hydrogen abstraction step generally occur with activation barriers lower than 100 kJ mol^{-1} (see Table 1), so that the reaction can be carried out at room temperature. The optimised transition state during C-H hydrogen abstraction is shown in Figure 5A. Attempts to include a further pyridine base in the transition state did not lower the activation barrier.

Using the calculated differences in free energies for the hydrogen abstraction transition step, the activation energy (E_A) barrier values were obtained and plotted as Boltzmann coefficients versus the experimentally measured chemical rate constants k_1 in Figure 5B. For all alcohols a reasonably good fit is observed, which suggests that all processes follow a similar reaction pathway with electronic factors dominating the H-atom transfer. The value for the experimental rate constant for benzyl alcohol appears slightly high, which may be in part due to an underlying direct background oxidation of benzyl alcohol at +1 V vs. SCE. Thus, the experimentally observed k_1 rate constant appears slightly high.

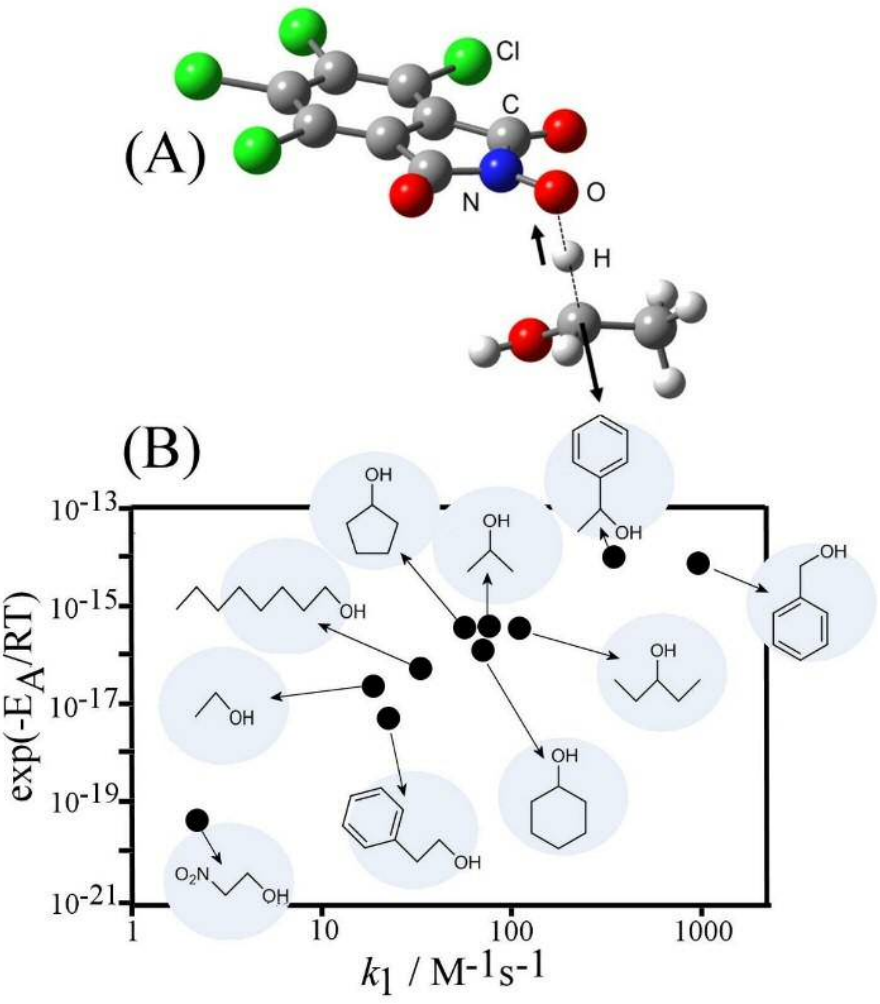

Figure 5. (A) Molecular structure of DFT calculated transition state for the hydrogen abstraction step between ethanol and Cl_4PINO (red: oxygen, blue: nitrogen, grey: carbon, white: hydrogen, green: chlorine; arrows: displacement vectors of the TS imaginary frequency). Image obtained with GaussView 5.0.8. (B) Plot (double logarithmic) of the activation factor $\exp(-E_A/RT)$ derived from DFT theory versus the experimental rate constant k_1.

Conclusion

An investigation of the reactivity of tetrachloro-phthalimido-*N*-oxyl (Cl_4PINO) generated electrochemically at the surface of a 3 mm diameter glassy carbon electrode has revealed some

new and potentially important quantitative insights into the mechanism during C-H atom abstraction reactions involving primary and secondary alcohols. The formation of the Cl_4PINO radical (in acetonitrile/1 M pyridine) is confirmed by *in situ* electrochemical EPR spectroscopy, but it is also shown that the radical is sensitive to slow decay induced by moisture. Cyclic voltammetry experiments can be employed to extract quantitative kinetic information such as rate constants for the C-H hydrogen abstraction process with ambient moisture levels in the acetonitrile solvent. The C-H hydrogen abstraction is shown to be of "EC'-type", but with only half of the redox mediator being re-generated directly at the electrode surface. This conclusion is reached from fitting a theory model to the plot of current versus alcohol concentration. It has to be kept in mind that alternative mechanistic schemes may give a similar fit. The suggested reaction scheme results in non-linear current *versus* substrate concentration plots with a plateau at high concentrations. These results have direct implication in the bulk scale synthetic application of Cl_4PINO, but will need further work to provide (i) better evidence for reaction intermediates and (ii) data for a broader spectrum of substrates. In future combined DFT and voltammetric analysis methods could be employed for the optimisation and prediction for a wider range of Cl_4PINO reactions.

ACKNOWLEDGMENT

A.B. thanks Roger and Sue Whorrod for a research fellowship and the University of Bath for high performance computing resources.

REFERENCES

[1] E.J. Horn, B.R. Rosen, Y. Chen, J.Z. Tang, K. Chen, M.D. Eastgate, P.S. Baran, *Nature* **2016**, *533*, 77–81.

[2] E.J. Horn, B.R. Rosen P.S. Baran, *ACS Central Sci.* **2016**, *2*, 302–308.

[3] L. Bauer, S.V. Miarka, *J. Amer. Chem. Soc.* **1957**, *79*, 1983–1985.

[4] W.R. Roderick, W.G. Brown, *J. Amer. Chem. Soc.* **1957**, *79*, 5196–5198.

[5] F. Minisci, F. Recupero, A. Cecchetto, C. Punta, C. Gambarotti, F. Fontana, G.F. Pedulli, *J. Heterocyclic Chem.* **2003**, *40*, 325–328.

[6] T. Shiraishi, Y. Sannami, H. Kamitakahara, T. Takano, *Electrochim. Acta* **2013**, *106*, 440–446.

[7] N.E. Khrushch, O.M. Chukanova, F.S. Dyachkovskii, V.A. Golubev, *Bull. Academy of Sci. USSR Div. Chem. Sci.* **1981**, *30*, 976–980.

[8] F. Recupero, C. Punta, *Chem. Rev.* **2007**, *107*, 3800–3842.

[9] P.L. Bragd, H. van Bekkum, A.C. Besemer, *Topics Catal.* **2004**, *27*, 49–66.

[10] S.D. Ahn, A. Kolodziej, R. Malpass-Evans, M. Carta, N.B. McKeown, S.D. Bull, A. Buchard, F. Marken, *Electrocatalysis* **2016**, *7*, 70–78.

[11] M. Rafiee, B. Karimi, S. Alizadeh, *ChemElectroChem* **2014**, *1*, 455–462.

[12] G. Biliuta, L. Fras, M. Drobota, Z. Persin, T. Kreze, K. Stana-Kleinschek, V. Ribitsch, V. Harabagiu, S. Coseri, *Carbohydrate Polym.* **2013**, *91*, 502–507.

[13] S.R. Waldvogel, M. Selt, *Angew. Chem. Int. Ed.* **2016**, *55*, 12578–12580.

[14] K. Sugamoto, Y.I. Matsushita, Y.H. Kameda, M. Suzuki, T. Matsui, *Synth. Commun*. **2005**, *35*, 67–70.

[15] C. Ueda, M. Noyama, H. Ohmori, M. Masui, *Chem. Pharm. Bull.* **1987**, *35*, 1372–1377.

[16] T. Shiraishi, T. Takano, H. Kamitakahara, F. Nakatsubo, *Holzforschung* **2012**, *66*, 311–316.

[17] K. Gorgy, J.C. Lepretre, E. Saint-Aman, C. Einhorn, J. Einhorn, C. Marcadal, J.L. Pierre, *Electrochim. Acta* **1998**, *44*, 385–393.

[18] S. Wertz, A. Studer, *Green Chem.* **2013**, *15*, 3116–3134.

[19] C. Einhorn, J. Einhorn, C. Marcadal, J.L. Pierre, *Chem. Commun.* **1997**, 447–448.

[20] F. Minisci, C. Punta, F. Recupero, F. Fontana, G.F. Pedulli, *Chem. Commun.* **2002**, 688–689.

[21] F. Minisci, F. Recupero, C. Punta, C. Gambarotti, F. Antonietti, F. Fontana, G.F. Pedulli, *Chem. Commun.* **2002**, 2496–2497.

[22] Q.H. Zhang, C. Chen, H. Ma, H. Miao, W. Zhang, Z.Q. Sun, J.J. Xu, *Chem. Technol. Biotechnol*. **2008**, *83*, 1364–1369.

[23] N. Koshino, Y. Cai, J.H. Espenson, *J. Phys. Chem. A* **2003**, *107*, 4262–4267.

[24] N. Koshino, B. Saha, J.H. Espenson, *J. Org. Chem.* **2003**, *68*, 9364–9370.

[25] C.R. Wilke, P. Chang, *AICHE J.* **1955**, *1*, 264–270.

[26] Gaussian 09, Revision D.01, M.J.Frisch, G.W. Trucks, H.B. Schlegel, G.E. Scuseria, M.A. Robb, J.R. Cheeseman, G. Scalmani, V. Barone, B. Mennucci, G.A. Petersson, H. Nakatsuji, M. Caricato, X. Li, H.P. Hratchian, A.F. Izmaylov, J. Bloino, G. Zheng, J.L. Sonnenberg, M. Hada, M. Ehara, K. Toyota, R. Fukuda, J. Hasegawa, M. Ishida, T. Nakajima, Y. Honda, O. Kitao, H. Nakai, T. Vreven, J.A. Montgomery Jr., J.E. Peralta, F. Ogliaro, M. Bearpark, J.J. Heyd, E.

Brothers, K.N. Kudin, V.N. Staroverov, R. Kobayashi, J. Normand, K. Raghavachari, A. Rendell, J.C. Burant, S.S. Iyengar, J. Tomasi, M. Cossi, N. Rega, J.M. Millam, M. Klene, J.E. Knox, J.B. Cross, V. Bakken, C. Adamo, J. Jaramillo, R. Gomperts, R.E. Stratmann, O. Yazyev, A.J. Austin, R. Cammi, C. Pomelli, J.W. Ochterski, R.L. Martin, K. Morokuma, V.G. Zakrzewski, G.A. Voth, P. Salvador, J.J. Dannenberg, S. Dapprich, A.D. Daniels, Ö. Farkas, J.B. Foresman, J.V. Ortiz, J. Cioslowski, D.J. Fox, Gaussian, Inc., Wallingford CT (2009)

[27] J.E.B. Randles, *Trans. Faraday Soc.* **1948**, *44*, 327–328.

[28] C. Annunziatini, M.F. Gerini, O. Lanzalunga, M. Lucarini, *J. Org. Chem.* **2004**, *69*, 3431–3438.

[29] I.B. Krylov, M.O. Kompanets, K.V. Novikova, I.O. Opeida, O.V. Kushch, B.N. Shelimov, G.I. Nikishin, D.O. Levitsky, A.O. Terent'ev, *J. Phys. Chem. A* **2016**, *120*, 68–73.

[30] H. Tsubomura, R.S. Mulliken, *J. Amer. Chem. Soc.* **1960**, *82*, 5966–5974.

[31] A. Moscatelli, M.F. Ottaviani, W. Adam, A. Buchachenko, S. Jockusch, N.J. Turro, *Helv. Chim. Acta* **2006**, *89*, 2441–2449.

[32] V. Chechik, H.J. Wellsted, A. Korte, B.C. Gilbert, H. Caldararu, P. Ionita, A. Caragheorgheopol, *Faraday Disc.* **2004**, *125*, 279–291.

[33] T.J. Stone, T. Buckman, P.L. Nordio, H.M. McConnell, *PNAS* **1965**, *54*, 1010–1011.

[34] S. Matsui, T. Fujita, *Catal. Today* **2001**, *71*, 145–152.

[35] E. Baciocchi, M.F. Gerini, O. Lanzalunga, *J. Org. Chem.* **2004**, *69*, 8963–8966.

[36] C. Ueda, M. Noyama, H. Ohmori, M. Masui, *Chem. Pharm. Bull.* **1987**, *35*, 1372–1377.

[37] N. Koshino, Y. Cai, J.H. Espenson, *J. Phys. Chem. A* **2003**, *107*, 4262–4267.

[38] N. Koshino, B. Saha, J.H. Espenson, *J. Org. Chem.* **2003**, *68*, 9364–9370.

[39] Y. Cai, N. Koshino, B. Saha, J.H. Espenson, *J. Org. Chem.* **2005**, *70*, 238–243.

[40] B. Saha, N. Koshino, J.H. Espenson, *J. Phys. Chem. A* **2004**, *108*, 425–431.

[41] A. Galano, J.R. Alvarez-Idaboy, M.E. Ruiz-Santoyo, A. Vivier-Bunge, *J. Phys. Chem. A* **2002**, *106*, 9520–9528.